ARTICLES

Journal of Semiconductors
(2022) 43, 092201
doi: 10.1088/1674-4926/43/9/092201

Defect passivation with potassium trifluoroborate for efficient spray-coated perovskite solar cells in air

Chen Gao, Hui Wang, Pang Wang, Jinlong Cai, Yuandong Sun, Cong Yu, Teng Li, Xiaoshuai Zhang, Dan Liu, and Tao Wang†

School of Materials Science and Engineering, Wuhan University of Technology, Wuhan 430070, China

Abstract: Defects as non-radiative recombination centers hinder the further efficiency improvements of perovskite solar cells (PSCs). Additive engineering has been demonstrated to be an effective method for defect passivation in perovskite films. Here, we employed (4-methoxyphenyl) potassium trifluoroborate ($C_7H_7BF_3KO$) with BF_3^- and K^+ functional groups to passivate spray-coated $(FAPbI_3)_x(MAPbBr_3)_{1-x}$ perovskite and eliminate hysteresis. It is shown that the F of BF_3^- can form hydrogen bonds with the H atom in the amino group of MA^+/FA^+ ions of perovskite, thus reducing the generation of MA^+/FA^+ vacancies and improving device efficiency. Meanwhile, K^+ and reduced MA^+/FA^+ vacancies can inhibit ion migration, thereby eliminating hysteresis. With the aid of $C_7H_7BF_3KO$, we obtained hysteresis-free PSCs with the maximum efficiency of 19.5% by spray-coating in air. Our work demonstrates that additive engineering is promising to improve the performance of spray-coated PSCs.

Key words: perovskite solar cells; spray-coating; additive engineering; defect passivation; hysteresis

Citation: C Gao, H Wang, P Wang, J L Cai, Y D Sun, C Yu, T Li, X S Zhang, D Liu, and T Wang, Defect passivation with potassium trifluoroborate for efficient spray-coated perovskite solar cells in air[J]. *J. Semicond.*, 2022, 43(9), 092201. https://doi.org/10.1088/1674-4926/43/9/092201

1. Introduction

Perovskite solar cells (PSCs) have shown great commercial potential, due to their high power conversion efficiency (PCE)[1, 2], low cost and solution- and air-based fabrication processes[3–7]. One of the challenges in the commercialization of PSCs is to scale them from the laboratory level to large area fabrication[8]. As the most commonly employed fabrication process in laboratory, spin coating has a low utilization of raw materials and cannot obtain uniform films in a large area[9–11]. With the advantages of fast deposition speed, high raw material utilization and compatibility with nonplanar surfaces, spray-coating has been demonstrated as a promising scalable film deposition process for the large area fabrication of PSCs[12, 13].

Spray coating PSCs with uniform perovskite films, controllable morphology and reproducible device performance has been the primary focus of research, and many approaches (e.g., hot-air blowing treatment[14], plasma treatment[15], low-vacuum treatment[16], anti-solvent bath treatment[17], and air knife treatment[18]) have been developed to this end. These post-treatment processes inevitably complicate the device preparation, increase cost, and fail to achieve high device performance due to the presence of intrinsic defects within the spray-coated perovskite layer[19]. The defects in perovskite structures, including vacancies, interstitials, and anti-site defects, are non-radiative recombination centers that impair device performance[19–21]. Among them, vacancy defects such as cation (MA^+/FA^+) vacancies and halogen (I^-) vacancies are most likely to occur due to their lowest formation energy[22]. Moreover, cation vacancies can induce other negatively charged defects, such as undercoordinated I^- and Pb-I anti-defects (PbI_3^-), further increasing the defect density in perovskite films[23]. Furthermore, vacancy defects provide channels for ion migration, which is considered to be one of the main reasons for device hysteresis[24–26].

Additive engineering is an efficient method to passivate defects in perovskite films[27]. Zhao *et al.* reported that the O atom in polyethylene glycol (PEG) additive can form a hydrogen bond with MA^+ in perovskite to stabilize MA^+[28]. Similarly, Li *et al.* used dipentaterythritol pentaacrylate (DPPA) additive to passivate vacancy defects, and the O and hydroxyl (–OH) groups of DPPA are suggested to form hydrogen bonds with FA^+ and I^- in perovskites respectively, thereby inhibiting the generation of vacancy defects[29]. The F atom of NaF has also been demonstrated to be able to form strong hydrogen bonds with MA^+/FA^+, thus passivating cation vacancies[30]. As a result, the incorporation of additives in perovskites has been found to reduce or eliminate device hysteresis, especially potassium salts such as KI, KI_3 and KPF_6, which is attributed to the effective inhibition of ion migration by K^+[31–35]. Additive engineering, without introducing any additional processing steps, is simple and convenient, and fully conforms to the characteristics of high throughput and fast deposition of spray-coating.

In this work, we employed (4-methoxyphenyl) potassium trifluoroborate ($C_7H_7BF_3KO$) as an additive to passivate defects in one-step spray-coated $(FAPbI_3)_x(MAPbBr_3)_{1-x}$ perovskite films to realize efficient devices without hysteresis. It is shown that hydrogen bonds can form between F in BF_3^- of $C_7H_7BF_3KO$ and H in the amino group of the perovskite cation MA^+/FA^+, thereby stabilizing MA^+/FA^+, inhibiting the occur of A-site cation vacancies, reducing non-radiative recom-

Correspondence to: T Wang, twang@whut.edu.cn
Received 19 APRIL 2022; Revised 2 MAY 2022.

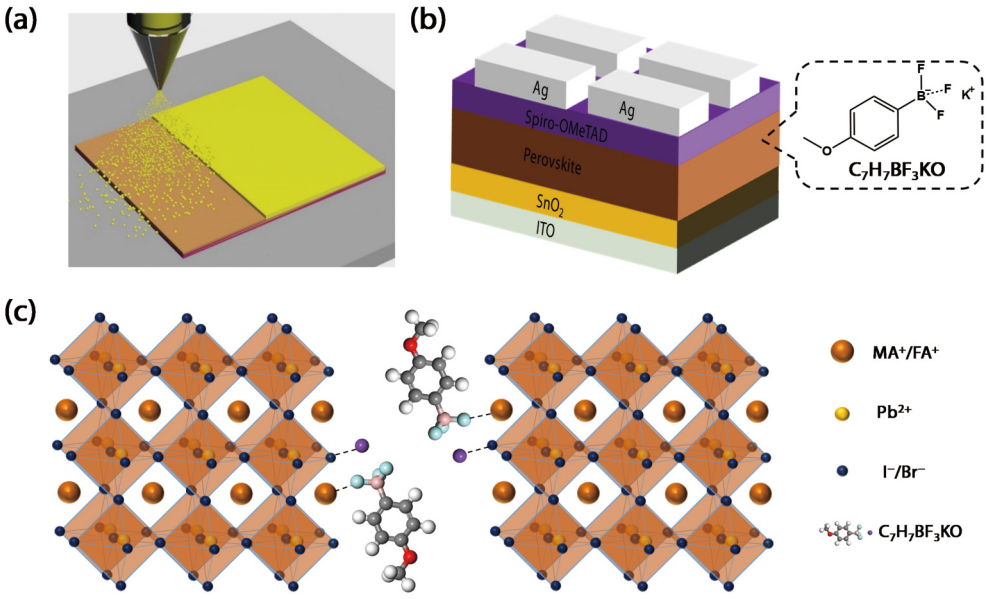

Fig. 1. (Color online) (a) Schematic diagram of one-step spray-coating perovskite films. (b) Structure of the spray-coated devices. (c) Schematic diagram of the action of $C_7H_7BF_3KO$.

bination and improving the performance of the device. Moreover, K^+ in $C_7H_7BF_3KO$ and the reduced MA^+/FA^+ vacancies due to hydrogen bonding interactions can suppress migration, thereby eliminating hysteresis. Ultimately, we obtained hysteresis-free spray-coated device with a maximum PCE (PCE_{max}) of *ca.* 19.5% from both forward and reverse scans. Our work demonstrates that defect passivation by additives engineering is an effective way to further improve the performance of spray-coated devices, paving the way for large-scale fabrication.

2. Experimental section

2.1. Material

Lead(II) iodide (PbI_2) was purchased from TCI. (4-methoxyphenyl) potassium trifluoroborate ($C_7H_7BF_3KO$) was purchased from Macklin. Thiourea (CH_4N_2S), γ-butyrolactone (GBL), tin(II) chloride dihydrate ($SnCl_2{\cdot}2H_2O$) and 4-tert-butylpyridine (TBP) were purchased from Aladdin. L-α-phosphatidylcholine (L-α-P), bis(trifluoromethane)sulfonimide lithium salt (Li-TFSI) and other solvents were purchased from Sigma-Aldrich. Other materials were all purchased from Xi'an Polymer Light Technology and used as received.

2.2. Device fabrication

The ITO glass was ultrasonically cleaned with deionization, ethanol and isopropanol in sequence for 15 min, and treated with UV-Ozone for 15 min. $SnCl_2{\cdot}2H_2O$ and CH_4N_2S were dissolved in deionized water in a molar ratio of 1 : 1 to obtain a SnO_2 solution with a concentration of 45 mg/mL. The SnO_2 solution was spin-coated onto ITO glass at 3000 rpm, then annealed at 200 °C for 1 h, and then treated with UV-Ozone for 40 min. PbI_2 (835 mg), FAI (238 mg), MABr (34 mg) and MACl (19 mg) were dissolved in a mixed solvent of DMSO (1950 μL), GBL (1950 μL) and IPA (100 μL). 0.02 wt% L-α-P and 0.5 wt% $C_7H_7BF_3KO$ were added to the perovskite precursor solution. Perovskite films were fabricated by Siansonic UC342 spray-coater and detailed spraying parameters are: the nitrogen flow pressure is 0.5 MPa, the substrate temperature is 60 °C, the flow rate is 0.7 mL/min, the height and moving speed of nozzle is 60 mm and 900 mm/min, the ambient relative humidity is less than 40% and the ambient temperature is about 25 °C. Then, the perovskite wet films were annealed at 150 °C for 25 min. In an N_2-filled glovebox, the Spiro-OMeTAD solution (95 mg/mL in CB) containing 30 μL TBP, 30 μL FK209 (400 mg/mL in acetonitrile) and 11.5 μL Li-TFSI (400 mg/mL in acetonitrile) were spin-coated onto spray-coated perovskite films at 4000 rpm. Ultimately, the Ag electrodes were evaporated onto Spiro-OMeTAD and the fabrication of devices is completed.

2.3. Characterization

Optical and AFM images were obtained by BX51 microscope (Olympus, Japan) and atomic force microscopy (NT-MDT, Russia), respectively. The light intensity of the Newport 3A solar simulator was calibrated with NREL certified silicon solar cells to 100 mW/cm^2, and *J–V* curves were obtained by using *J–V* scanning software of Ossila Ltd. (UK) and 2612B source meter unit of Keithley (USA). EQE measurements were carried out by EQE system (Zolix, China). ^{1}H NMR spectra were measured by ^{1}H NMR spectrometer (DRX500, Bruker, Germany). XRD spectra were obtained by X-ray diffractometer (D8 Advance, Bruker, Germany). UV–vis absorption was measured by UV–vis spectrophotometer (Hitachi U-3900H, Japan). PL spectra were obtained by PL microscopic spectrometer (Flex One, Zolix, China). TRPL decay curves were obtained through a time-correlated single photon counting spectrofluorometer (PicoQuant, Germany). Mott-Schottky plots and EIS measurements were conducted through ModuLab XM electrochemical workstation (AMETEK, UK). Equivalent circuit simulations were carried out by the ZView software package (Scribner, USA).

3. Results and discussion

The $(FAPbI_3)_x(MAPbBr_3)_{1-x}$ perovskite active layers were fabricated by one-step spray-coating in air (Fig. 1(a)), using precursors described in the experimental section, where surfactant L-α-phosphatidylcholine (L-α-P) was incorporated be-

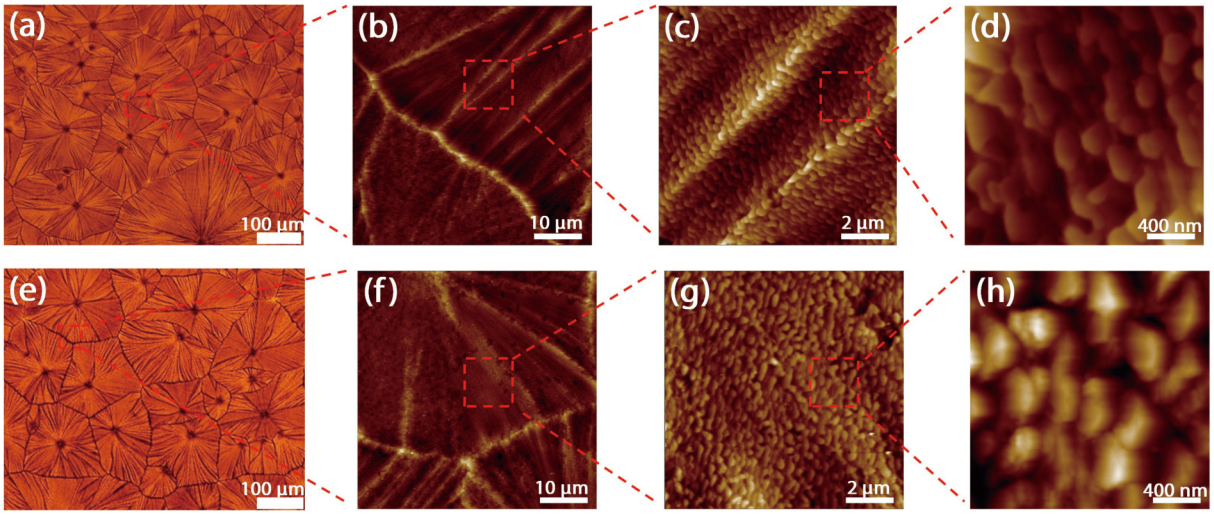

Fig. 2. (Color online) The optical images of (a) reference and (e) $C_7H_7BF_3KO$ based spray-coated perovskite films. The AFM images of (b–d) reference and (f–h) $C_7H_7BF_3KO$ based spray-coated perovskite films at different magnifications.

cause it is critical to adjust the surface energy to receive uniform perovskite films during spray coating[36, 37]. However, serious hysteresis exist in the L-α-P modified PSCs[37]. We have demonstrated that a secondary additive KI can help to reduce hysteresis of spray-coated PSCs, although it cannot completely eliminate hysteresis[37]. $C_7H_7BF_3KO$ was chosen in this work as a defect passivator for the spray-coated PSCs (Figs. 1(b) and 1(c)). The morphology of spray-coated perovskite films with or without the presence of $C_7H_7BF_3KO$ were first examined and shown in Fig. 2. The optical images (Figs. 2(a) and 2(e)) show that the grain sizes of the reference and $C_7H_7BF_3KO$ based perovskite films are similar of over 100 μm in diameter. However, further morphology characterization using atomic force microscopy (AFM) in smaller scale shows that the spray-coated perovskite films are hierarchical, with the large grains observed in Figs. 2(b)–2(d) and 2(f)–2(h) being composed of small grains of *ca.* 400 nm in diameter, which is consistent with our previous report[37]. The introduction of $C_7H_7BF_3KO$ brings no apparent changes to the size of both large- and small- grains. However, the $C_7H_7BF_3KO$ based perovskite film (Fig. 2(h)) shows a smoother surface with a lower root-mean-square (RMS) roughness of 18.8 nm, compared to 27.0 nm for the reference film (Fig. 2(d)), which is conducive to improving the interface contact.

The X-ray diffraction (XRD) patterns in Fig. 3(a) show that, compared with the reference perovskite film, the $C_7H_7BF_3KO$ based perovskite film displays stronger diffraction peak intensities at 13.9°, 28.1°, 31.5°, 40.2° and 42.8°, which correspond to the (110), (220), (310), (224) and (330) crystal plane of perovskite, respectively. The enhancement of peak intensity represents the increased crystallinity, which is conducive to enhance the light absorption of perovskite films and improve the performance of the device[38]. There are no new peaks or peak shifts, indicating that the perovskite phase structure remains consistent and $C_7H_7BF_3KO$ cannot enter the perovskite lattice[39]. The UV–vis absorption spectra (Fig. 3(b)) confirm the slightly better absorption ability of the $C_7H_7BF_3KO$ based perovskite film, especially at the wavelength of 450–550 nm. The steady-state PL spectra is shown in Fig. 3(c), the PL intensity of $C_7H_7BF_3KO$ based perovskite film is significantly enhanced compared with the reference film, indicating that

Table 1. The fitting parameters of TRPL for reference and $C_7H_7BF_3KO$ based spray-coated perovskite films.

Additive	τ_1 (ns)	A_1 (%)	τ_2 (ns)	A_2 (%)	τ_{ave} (ns)
w/o	100	39	266	61	201
$C_7H_7BF_3KO$	140	33	370	67	294

$C_7H_7BF_3KO$ effectively passivates the defects and non-radiative recombination is significantly suppressed[40, 41]. The time-resolved photoluminescence (TRPL) decay curves (Fig. 3(d)) of spray-coated perovskite films show bi-exponential decays. The decay curves are fitted by the equation: $i = A_1\exp(-t/\tau_1)+A_2\exp(-t/\tau_2)$, where τ_1 is the fast decay time associated with trap-assisted non-radiative recombination, τ_2 is the slow decay time related to bimolecular radiative recombination, A_1 and A_2 are decay amplitudes[42, 43]. The detailed fitting parameters are shown in Table 1. With the incorporation of $C_7H_7BF_3KO$, the values of τ_1 and τ_2 both increased, and the average PL lifetime was improved from 201 to 294 ns. This longer carrier lifetime further demonstrates the lower trap density and improved quality of spray-coated perovskite films after passivation by $C_7H_7BF_3KO$[44].

The hydrogen bonding interactions between $C_7H_7BF_3KO$ and the cation MA^+/FA^+ in perovskite were investigated through ^1H nuclear magnetic resonance (^1H NMR) spectra. As shown in Figs. 3(e)–3(f), after the addition of $C_7H_7BF_3KO$, the chemical shifts (δ) of H of $-NH_2^+$ in FAI and $-NH_3^+$ in MABr move from 8.78 and 7.67 ppm to 8.67 and 7.56 ppm respectively as a result of the formation of hydrogen bonds, which agrees with literature reports[28, 29]. The H of $-OCH_3$ in $C_7H_7BF_3KO$ has no chemical shift, indicating that O is not involved in the formation of hydrogen bonds. Therefore, we think that the F in BF_3^- can form hydrogen bonds with the H on the amino group in MA^+/FA^+, which can effectively stabilize organic cations, reduce the generation of A-site vacancies, thereby improving the performance of the spray-coated devices[30].

The PSC devices fabricated in this work have an n-i-p structure of ITO/SnO_2/Perovskite/Spiro-OMeTAD/Ag. The effects of $C_7H_7BF_3KO$ on the photovoltaic performance of spray-coated PSCs are shown in Fig. 4(a) and Table 2. The optimization pro-

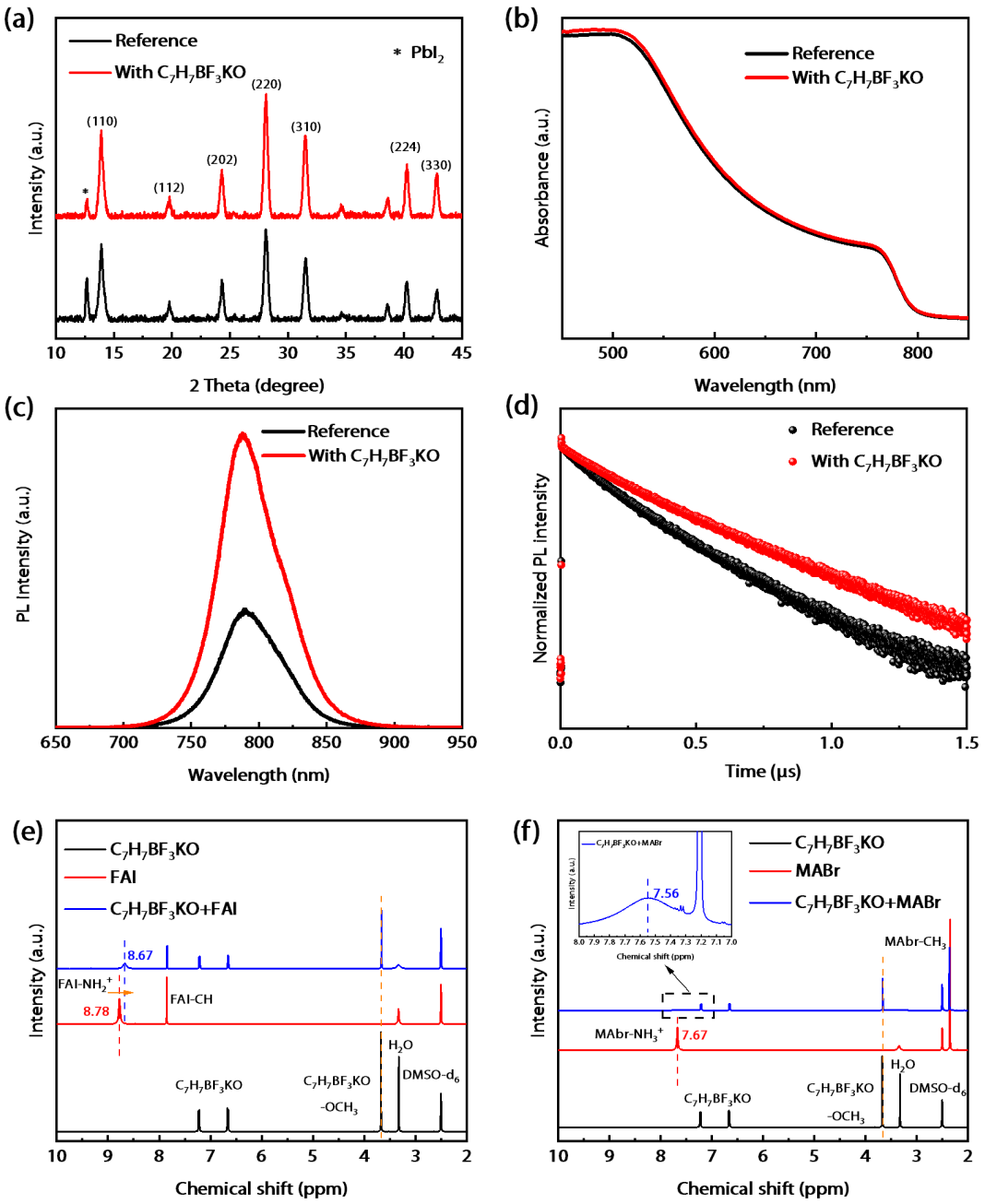

Fig. 3. (Color online) (a) XRD patterns, (b) UV–vis absorption spectra, (c) steady-state PL spectra and (d) TRPL decay curves of reference and $C_7H_7BF_3KO$ based spray-coated perovskite films. ^1H NMR spectra of (e) FAI, $C_7H_7BF_3KO$ and FAI-$C_7H_7BF_3KO$ mixture and (f) MABr, $C_7H_7BF_3KO$ and MABr-$C_7H_7BF_3KO$ mixture in DMSO-d6 solution.

Table 2. Summary of photovoltaic performance parameters of the reference and $C_7H_7BF_3KO$ based spray-coated PSCs.

Additive	Scan direction	PCE_{max} (PCE_{ave}) (%)	FF (FF_{ave}) (%)	J_{SC} (J_{SCave}) (mA/cm^2)	V_{OC} (V_{OCave}) (V)
w/o	reverse	16.3 (14.7 ± 1.1)	67.1 (62.0 ± 3.9)	21.9 (21.6 ± 0.5)	1.11 (1.09 ± 0.02)
	forward	14.9 (12.6 ± 1.2)	61.6 (53.8 ± 4.5)	21.9 (21.8 ± 0.5)	1.11 (1.07 ± 0.02)
$C_7H_7BF_3KO$	reverse	19.4 (17.6 ± 0.8)	77.4 (72.4 ± 2.5)	22.0 (21.8 ± 0.3)	1.14 (1.11 ± 0.01)
	forward	19.5 (17.6 ± 0.9)	77.8 (72.6 ± 3.1)	22.0 (21.9 ± 0.3)	1.14 (1.11 ± 0.01)

cess of the additive amount of $C_7H_7BF_3KO$ is shown in Table S1, from which the optimum content of 0.5 wt% of $C_7H_7BF_3KO$ can be determined. The PCE_{max} of the reference device is 16.3% with a fill factor (FF) of 67.1%, a short-circuit current density (J_{SC}) of 21.9 mA/cm^2 and an open-circuit voltage (V_{OC}) of 1.11 V. After the addition of 0.5 wt% $C_7H_7BF_3KO$, the average PCE (PCE_{ave}) of PSCs increases significantly from 14.7% to 17.6%. The PCE of $C_7H_7BF_3KO$ based champion device reaches 19.5%, with the improvement mainly attributing to enhanced FF and V_{OC}, reaching 77.8% and 1.14 V, respectively. The steady-state power output of the spray-coated devices at the maximum power point (MPP) is shown in Fig. S1. The PCE of the reference device shows a gradual decrease with time that finally stabilizes at 15.2%, which is likely caused by hysteresis[45], whilst the PCE of the $C_7H_7BF_3KO$ based device stabilizes at 18.9% for the whole duration of

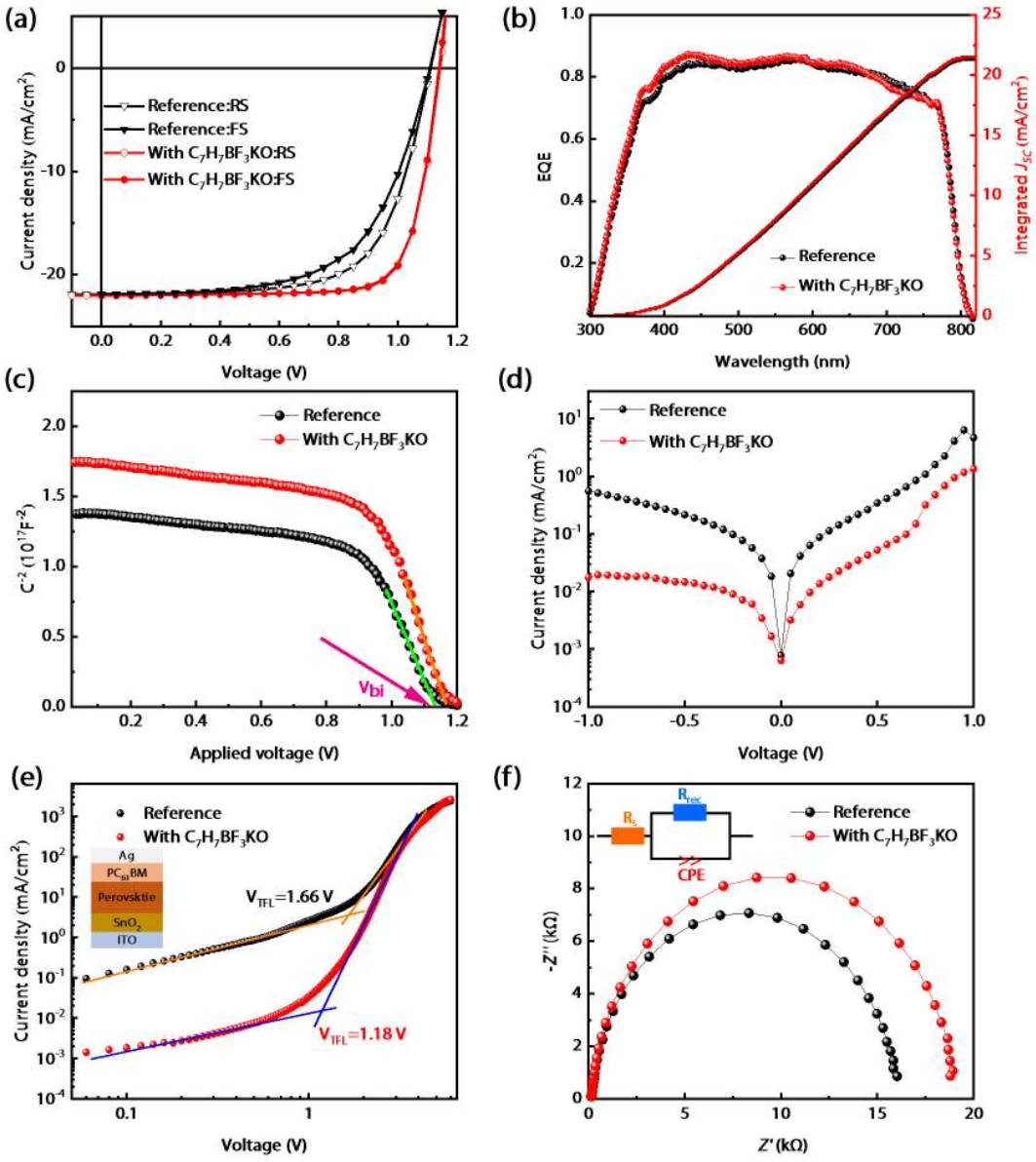

Fig. 4. (Color online) (a) *J–V* curves of the reference and $C_7H_7BF_3KO$ based spray-coated PSCs. (b) EQE spectra and corresponding integrated J_{SC}. (c) Mott–Schottky plots and (d) dark *J–V* curves of PSCs. (e) The SCLC curves of electron-only devices. (f) Nyquist plots of PSCs.

the MPP testing. The hysteresis indices (HI = ($PCE_{reverse}$ – PCE_{forwad})/$PCE_{reverse}$) for the reference and $C_7H_7BF_3KO$ based devices are 8.6% and 0.5%, respectively, indicating that hysteresis is negligible with the presence of $C_7H_7BF_3KO$. This is attributed to the effect of K^+ and hydrogen bond-stabilized MA^+/FA^+, which effectively suppresses ion migration and eliminates hysteresis[31–35]. Fig. 4(b) shows the external quantum efficiency (EQE) spectra of the champion devices. The corresponding integrated J_{sc} values of the reference and $C_7H_7BF_3KO$ based devices are 21.3 and 21.5 mA/cm^2 respectively, which are close to the values obtained from the *J–V* curves, demonstrating the accuracy of *J–V* measurements.

We then studied the optoelectronic properties of PSCs with and without $C_7H_7BF_3KO$ to explain *J–V* performance improvement. The built-in potential (V_{bi}) of PSCs can be obtained from Mott–Schottky curves (Fig. 4(c)), the value of V_{bi} for the reference and $C_7H_7BF_3KO$ based PSCs are 1.13 and 1.17 V, respectively. The enhanced built-in potential provides a larger driving force for charge transport and collection, resulting in reduced carrier recombination and higher V_{OC}[46, 47]. In addition, the dark *J–V* curves of devices are shown in Fig. 4(d), compared with the reference PSC, the dark current density of $C_7H_7BF_3KO$ based PSC is reduced by one order of magnitude. The reduction of leakage current density indicates a lower defect density that contributes to a higher FF, which further confirms the passivation effect of $C_7H_7BF_3KO$[48, 49].

We then carried out space charge limited current (SCLC) measurements (Fig. 4(e)) based on electron-only devices with a structure of ITO/SnO_2/perovskite/$PC_{61}BM$/Ag to evaluate the trap density of devices with and without $C_7H_7BF_3KO$. The trap density can be estimated by the equation $n_t = 2\varepsilon\varepsilon_0 V_{TFL}/eL^2$, where V_{TFL} is trap-filled limit voltage defined as the intersection voltage between the Ohmic-type response region and the trap-filled limit region, ε_0 is the vacuum permittivity, ε represents the relative dielectric constant, L means the film thickness (*ca.* 600 nm), and e refers to elementary charge of the electron[50–52]. Compared with the reference device, the $C_7H_7BF_3KO$ based device exhibits a reduced V_{TFL} from 1.66 to 1.18 V, and the calculated trap densities are 1.63 × 10^{16} and 1.16 × 10^{16} cm^{-3}, respectively, indicating that the de-

Table 3. The fitting parameters of EIS for reference and $C_7H_7BF_3KO$-based spray-coated perovskite devices.

Additive	R_s (Ω·cm^2)	R_{rec} (Ω·cm^2)	CPE-T (F/cm^2)	CPE-P
w/o	156	15 886	9.80×10^{-9}	0.93
$C_7H_7BF_3KO$	136	18 972	7.62×10^{-9}	0.93

fects of PSCs are reduced after the introduction of $C_7H_7BF_3KO$. Therefore, the non-radiative recombination is effectively suppressed and the power conversion performance of PSC is enhanced[53].

Finally, the electrochemical impedance spectroscopy (EIS) was measured under dark conditions at a voltage bias of 1 V to evaluate charge transport in PSCs. The Nyquist plots are shown in Fig. 4(f), and the series resistance (R_s) and recombination resistance (R_{rec}) can be obtained by fitting with the inserted equivalent circuit model and the fitting parameters are shown in Table 3. After the incorporation of $C_7H_7BF_3KO$, the PSC displays a decreased R_s from 156 to 136 Ω cm^2, and an increased R_{rec} from 15 886 to 18 972 Ω·cm^2, indicating more efficient charge transport and decreased carrier recombination, which resulted in improved device performance[50, 54].

4. Conclusion

In conclusion, we have employed $C_7H_7BF_3KO$ as an additive to passivate defects in spray-coated perovskite films for high photovoltaic performance. The F of $C_7H_7BF_3KO$ forms hydrogen bonds with MA^+/FA^+ in perovskite to stabilize A-site cations and suppress the formation of cation vacancies, thereby reducing defect density and improving devices performance. Further, K^+ of $C_7H_7BF_3KO$ and reduced cation vacancies as a result of hydrogen bonding interactions can inhibit ion migration and eliminate hysteresis. The passivation of $C_7H_7BF_3KO$ enables us to fabricate efficient and hysteresis-free spray-coated PSCs with a PCE_{max} of 19.5% in air. Our work demonstrates that simple and convenient additive engineering has huge potential for improving the quality of spray-coated perovskite films, providing a feasible scheme to further improve the optoelectronic properties of spray-coated PSCs.

Acknowledgements

The authors acknowledge funding supports from the National Natural Science Foundation of China (51861145101).

Appendix A. Supplementary materials

Supplementary materials to this article can be found online at https://doi.org/10.1088/1674-4926/43/9/092201.

References

[1] Kojima A, Teshima K, Shirai Y, et al. Organometal halide perovskites as visible-light sensitizers for photovoltaic cells. J Am Chem Soc, 2009, 131, 6050

[2] NREL, Best Research-Cell Efficiency Chart. https://www.nrel.gov/pv/cell-efficiency.html (last access, January 26, 2022)

[3] Zhao D W, Dai S J, Li M, et al. Improved efficiency and stability of perovskite solar cells using a difluorobenzothiadiazole-based interfacial material. ACS Appl Energy Mater, 2021, 4, 10646

[4] Zhang H K, Chen Z L, Qin M C, et al. Multifunctional crosslinking-enabled strain-regulating crystallization for stable, efficient α-$FAPbI_3$-based perovskite solar cells. Adv Mater, 2021, 33, e2008487

[5] Mo Y P, Wang C, Zheng X T, et al. Nitrogen-doped tin oxide electron transport layer for stable perovskite solar cells with efficiency over 23%. Interdiscip Mater, 2022, 1, 309

[6] Zhang L X, Pan X Y, Liu L, et al. Star perovskite materials. J Semicond, 2022, 43, 030203

[7] Cheng Y H, Xu X W, Xie Y M, et al. 18% high-efficiency air-processed perovskite solar cells made in a humid atmosphere of 70% RH. Sol RRL, 2017, 1, 1770131

[8] Cheng Y H, So F, Tsang S W. Progress in air-processed perovskite solar cells: From crystallization to photovoltaic performance. Mater Horiz, 2019, 6, 1611

[9] Su J, Cai H K, Yang J T, et al. Perovskite ink with an ultrawide processing window for efficient and scalable perovskite solar cells in ambient air. ACS Appl Mater Interfaces, 2020, 12, 3531

[10] Uličná S, Dou B J, Kim D H, et al. Scalable deposition of high-efficiency perovskite solar cells by spray-coating. ACS Appl Energy Mater, 2018, 1, 1853

[11] Zuo C T, Vak D, Angmo D C, et al. One-step roll-to-roll air processed high efficiency perovskite solar cells. Nano Energy, 2018, 46, 185

[12] Guo A Z, Chou L H, Yang S, et al. Ultrasonic spray-coatings: Multichannel pumped ultrasonic spray-coating for high-throughput and scalable mixed halide perovskite solar cells. Adv Mater Interfaces, 2021, 8, 2170023

[13] Bishop J E, Smith J A, Lidzey D G. Development of spray-coated perovskite solar cells. ACS Appl Mater Interfaces, 2020, 12, 48237

[14] Su J, Cai H K, Ye X F, et al. Efficient perovskite solar cells prepared by hot air blowing to ultrasonic spraying in ambient air. ACS Appl Mater Interfaces, 2019, 11, 10689

[15] Hilt F, Hovish M Q, Rolston N, et al. Rapid route to efficient, scalable, and robust perovskite photovoltaics in air. Energy Environ Sci, 2018, 11, 2102

[16] Bishop J E, Smith J A, Greenland C, et al. High-efficiency spray-coated perovskite solar cells utilizing vacuum-assisted solution processing. ACS Appl Mater Interfaces, 2018, 10, 39428

[17] Cai H K, Liang X J, Ye X F, et al. High efficiency over 20% of perovskite solar cells by spray coating via a simple process. ACS Appl Energy Mater, 2020, 3, 9696

[18] Cassella E J, Spooner E L K, Thornber T, et al. Gas-assisted spray coating of perovskite solar cells incorporating sprayed self-assembled monolayers. Adv Sci, 2022, 9, e2104848

[19] Zhang F, Zhu K. Additive engineering for efficient and stable perovskite solar cells. Adv Energy Mater, 2020, 10, 1902579

[20] Fu L, Li H, Wang L, et al. Defect passivation strategies in perovskites for an enhanced photovoltaic performance. Energy Environ Sci, 2020, 13, 4017

[21] Gao F, Zhao Y, Zhang X W, et al. Recent progresses on defect passivation toward efficient perovskite solar cells. Adv Energy Mater, 2020, 10, 1902650

[22] Chen B, Rudd P N, Yang S, et al. Imperfections and their passivation in halide perovskite solar cells. Chem Soc Rev, 2019, 48, 3842

[23] Byranvand M M, Saliba M. Defect passivation of perovskite films for highly efficient and stable solar cells. Sol RRL, 2021, 5, 2100295

[24] Wu F, Pathak R, Qiao Q Q. Origin and alleviation of J-V hysteresis in perovskite solar cells: A short review. Catal Today, 2021, 374, 86

[25] Liu P Y, Wang W, Liu S M, et al. Fundamental understanding of photocurrent hysteresis in perovskite solar cells. Adv Energy Mater, 2019, 9, 1803017

[26] Ren X X, Zhang L X, Yuan Y B, et al. Ion migration in perovskite solar cells. J Semicond, 2021, 42, 010201

[27] Xiong S B, Hou Z Y, Zou S J, et al. Direct observation on p- to n-type transformation of perovskite surface region during defect pas-

sivation driving high photovoltaic efficiency. Joule, 2021, 5, 467
[28] Zhao Y C, Wei J, Li H, et al. A polymer scaffold for self-healing perovskite solar cells. Nat Commun, 2016, 7, 10228
[29] Li X D, Ke S Z, Feng X X, et al. Enhancing the stability of perovskite solar cells through cross-linkable and hydrogen bonding multifunctional additives. J Mater Chem A, 2021, 9, 12684
[30] Li N X, Tao S X, Chen Y H, et al. Cation and anion immobilization through chemical bonding enhancement with fluorides for stable halide perovskite solar cells. Nat Energy, 2019, 4, 408
[31] Abdi-Jalebi M, Andaji-Garmaroudi Z, Pearson A J, et al. Potassium- and rubidium-passivated alloyed perovskite films: Optoelectronic properties and moisture stability. ACS Energy Lett, 2018, 3, 2671
[32] Abdi-Jalebi M, Andaji-Garmaroudi Z, Cacovich S, et al. Maximizing and stabilizing luminescence from halide perovskites with potassium passivation. Nature, 2018, 555, 497
[33] Zheng F, Chen W J, Bu T L, et al. Triggering the passivation effect of potassium doping in mixed-cation mixed-halide perovskite by light illumination. Adv Energy Mater, 2019, 9, 1901016
[34] Zhang M, Bing J M, Cho Y, et al. Synergistic effect of potassium and iodine from potassium triiodide complex additive on gas-quenched perovskite solar cells. Nano Energy, 2019, 63, 103853
[35] Bu T L, Li J, Li H Y, et al. Lead halide-templated crystallization of methylamine-free perovskite for efficient photovoltaic modules. Science, 2021, 372, 1327
[36] Deng Y H, Zheng X P, Bai Y, et al. Surfactant-controlled ink drying enables high-speed deposition of perovskite films for efficient photovoltaic modules. Nat Energy, 2018, 3, 560
[37] Gao C, Wang P, Wang H, et al. Binary additive engineering enables efficient perovskite solar cells via spray-coating in air. ACS Appl Energy Mater, 2021, 4, 11496
[38] Koo D, Cho Y, Kim U, et al. High-performance inverted perovskite solar cells with operational stability via n-type small molecule additive-assisted defect passivation. Adv Energy Mater, 2020, 10, 2001920
[39] Zhao M, Yan J, Yu G, et al. Grain boundary defects passivated with tert-butyl methacrylate for high-efficiency perovskite solar cells. ACS Appl Energy Mater, 2021, 4, 11298
[40] Wang H H, Wang Z W, Yang Z, et al. Ligand-modulated excess PbI_2 nanosheets for highly efficient and stable perovskite solar cells. Adv Mater, 2020, 32, 2000865
[41] Wang A L, Wang J W, Niu X B, et al. Inhibiting octahedral tilting for stable $CsPbI_2Br$ solar cells. InfoMat, 2022, 4, e12263
[42] Hou M N, Xu Y Z, Zhou B, et al. Aryl diammonium iodide passivation for efficient and stable hybrid organ-inorganic perovskite solar cells. Adv Funct Mater, 2020, 30, 2002366
[43] Wu X Y, Jiang Y, Chen C, et al. Stable triple cation perovskite precursor for highly efficient perovskite solar cells enabled by interaction with 18C6 stabilizer. Adv Funct Mater, 2020, 30, 1908613
[44] Gao X X, Luo W, Zhang Y, et al. Stable and high-efficiency methylammonium-free perovskite solar cells. Adv Mater, 2020, 32, e1905502
[45] Rao Y, Li Z P, Liu D C, et al. Dual-functional additive to simultaneously modify the interface and grain boundary for highly efficient and hysteresis-free perovskite solar cells. ACS Appl Mater Interfaces, 2021, 13, 20043
[46] Chen Y L, Zuo X J, He Y Y, et al. Dual passivation of perovskite and SnO_2 for high-efficiency $MAPbI_3$ perovskite solar cells. Adv Sci, 2021, 8, 2001466
[47] Sha Y M, Bi E B, Zhang Y, et al. A scalable integrated dopant-free heterostructure to stabilize perovskite solar cell modules. Adv Energy Mater, 2021, 11, 2003301
[48] Wang Y, Chen G Y, Ouyang D, et al. High phase stability in $CsPbI_3$ enabled by Pb-I octahedra anchors for efficient inorganic perovskite photovoltaics. Adv Mater, 2020, 32, 2000186
[49] Li X, Sheng W, Duan X, et al. Defect passivation effect of chemical groups on perovskite solar cells. ACS Appl Mater Interfaces, 2021, in press
[50] Liu X X, Cheng Y H, Tang B S, et al. Shallow defects levels and extract detrapped charges to stabilize highly efficient and hysteresis-free perovskite photovoltaic devices. Nano Energy, 2020, 71, 104556
[51] Yuan J F, Bi C H, Wang S X, et al. Spray coating technologies: Spray-coated colloidal perovskite quantum dot films for highly efficient solar cells. Adv Funct Mater, 2019, 29, 1970337
[52] Dong Q F, Fang Y J, Shao Y C, et al. Solar cells. Electron-hole diffusion lengths > 175 μm in solution-grown $CH_3NH_3PbI_3$ single crystals. Science, 2015, 347, 967
[53] Ye F H, Ma J J, Chen C, et al. Roles of MACl in sequentially deposited bromine-free perovskite absorbers for efficient solar cells. Adv Mater, 2021, 33, e2007126
[54] Wang S J, Yang B W, Han J, et al. Polymeric room-temperature molten salt as a multifunctional additive toward highly efficient and stable inverted planar perovskite solar cells. Energy Environ Sci, 2020, 13, 5068

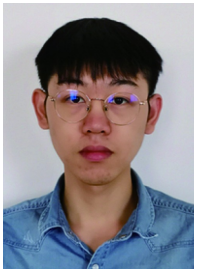

Chen Gao received his B.Sc. in Polymer Materials and Engineering at Wuhan University of Technology. He is currently a graduate student under the supervision of Prof. Tao Wang in the School of Material Science and Engineering, Wuhan University of Technology. His research focuses on the fabrication of perovskite solar cells via spray-coating.

Tao Wang received his B.Sc. in Polymer Materials (2002) and M.Sc. in Materials Science (2005). He obtained his Ph.D. in Soft Condensed Matter Physics from the University of Surrey (UK) in 2009, and then worked as a post-doc at the University of Sheffield (UK). He became a professor at Wuhan University of Technology (China) in 2013, and was admitted as a Fellow of the Royal Society of Chemistry (FRSC) in 2019. His research interests are optoelectronic materials and devices.